



A coupling framework for impact-induced progressive collapse analysis of RC frame structures

Yun Zhou^a, Ting Li^b, Fan Yi^{b,*}, Fei-Fan Feng^c, Jing-Ming Sun^d, Wei-Jian Yi^a

^a College of Civil Engineering, Hunan Provincial Key Lab on Damage Diagnosis for Engineering Structures, Hunan University, Changsha, 410082, China

^b College of Civil Engineering, Hunan University, Changsha, 410082, China

^c College of Civil Engineering, Hunan University of Science and Technology, Xiangtan, 411201, China

^d School of Civil Engineering, Qingdao University of Technology, Qingdao, 266033, China

ARTICLE INFO

Keywords:

Progressive collapse
Impact-induced column removal
RC frame structure
Numerical study
Energy balance method

ABSTRACT

The progressive collapse resistance of reinforced concrete (RC) frame structures under impact-induced column removal (ICR) is a critical yet underexplored area in structural engineering. This study proposes a novel coupling framework to integrate the impact response of frame columns with the progressive collapse behavior of RC frame structures. Utilizing validated finite element (FE) models, the framework employs the resistance curve of frame structures as a boundary condition for analyzing the downward pulling force exerted by impacted columns. This force is then applied as a time-varying external load to evaluate the progressive collapse response of frame substructures. Results demonstrate that the proposed framework achieves consistent displacement responses at beam-column joints compared to direct ICR analysis. The downward pulling force significantly amplifies structural deformation, increasing collapse risk compared to nominal column removal (NCR). Additionally, an approximate dynamic analysis method based on the work-energy principle is introduced to assess progressive collapse resistance under impact loading. The findings underscore the importance of considering impact effects in progressive collapse analysis, offering practical insights for safer structural design.

1. Introduction

Progressive collapse usually refers to the chain reaction of damage propagating along structural members and ultimately leading to overall or disproportionately large collapse of structures compared to the initial local damage [1], which is usually triggered by extreme loading effects like explosion, impact, and fire. Typical progressive collapse examples include the collapse of the Ronan Point apartment caused by a gas explosion [2], the collapse of the Alfred P. Murrah Federal Building due to an explosive terrorist attack [3], and the collapse of the World Trade Center caused by combined actions of impact and fire [4]. The catastrophic consequences of progressive collapse in building structures, despite their extremely low probabilities, have earned remarkable attention across various structural forms including RC frame structures.

Current codes concerning progressive collapse [5–7] mainly adopt the tie force method, enhanced local resistance method, and

* Corresponding author.

E-mail addresses: zhouyun05@hnu.edu.cn (Y. Zhou), litingli@hnu.edu.cn (T. Li), yifance@hnu.edu.cn (F. Yi), fengfeifan@hnust.edu.cn (F.-F. Feng), sunjingming@hnu.edu.cn (J.-M. Sun), wjyi@hnu.edu.cn (W.-J. Yi).

<https://doi.org/10.1016/j.job.2025.112517>

Received 29 December 2024; Received in revised form 10 March 2025; Accepted 29 March 2025

Available online 4 April 2025

2352-7102/© 2025 Elsevier Ltd. All rights are reserved, including those for text and data mining, AI training, and similar technologies.

alternate path method. Among them, the nominal column removal (NCR) relying on event-independent assumptions is widely adopted, i.e., neglecting the cause of initial local damage and focusing instead on load redistribution and resistance mechanisms after the removal of vertical load-bearing members. Based on the research method of NCR, Yi et al. [8] conducted a pseudo-static test on a planar frame substructure to investigate the progressive collapse resistance mechanisms and proposed the paradigm of relevant experiments. In the test, the removal process of mid-columns on the ground floor was simulated by the static unloading of a mechanical jack, and an electro-hydraulic servo actuator applied the gravity load of the superstructure acting on the mid-column of the top floor in a force-controlled manner. Qian et al. [9] evaluated the influence of seismic reinforcement on the progressive collapse resistance of RC frame structures through a pseudo-static pushdown test on beam-column substructures. Pham et al. [10] studied the influence of inertia and strain rate effects on the structural response through a sudden column removal test on a planar frame, which exhibited noticeable differences on damage and failure modes under dynamic and static conditions, respectively. Accidental actions on structures could trigger simultaneous failures of multiple columns. Therefore, some scholars [11–13] investigated the aftermath of multi-column removal on RC building structures. In addition, some scholars [14–16] found that the floor slabs and infill walls play positive roles in enhancing the progressive collapse resistance.

Although a large number of studies have investigated resistance mechanisms of structures under the event-independent assumption using NCR, the progressive collapse in actual scenarios is a complex mechanical behavior of structural systems, involving the uncertainty of extreme loads, the strong dynamic nonlinearity of structural behavior, and the large deformation characteristics of load-bearing mechanisms [17]. This highlights a critical gap in these previous studies: the neglect of the complicated interactions between extreme loads and the progressive collapse response of structures. Therefore, the progressive collapse resistance under specific extreme loads has received certain attentions. Li et al. [18] and Liu et al. [19] studied the differences of failure modes and resistance mechanisms of structures before and after the fire. Yu et al. [20] conducted dynamic experiments on columns subjected to contact detonations, which resulted in the uplift and out-of-plane action of substructures. Sun et al. [21] conducted a blasting demolition test on an 11-story frame structure, in which the data showed a large tensile force in the column section when the column subjected to the near-field explosion.

It should be particularly noted that, although impact events have long been recognized as a primary trigger for progressive collapse [22], experimental research remains limited. Previous studies using light gas guns [23] or hammer impacts [24] to remove temporary supports still fall under "event-independent" tests, as these supports cannot transmit tensile forces. Recent substructure tests on ICR [25] have revealed that the impacted column exerts a downward pulling force on the superstructure, resulting in significantly greater damage and displacements compared to "event-independent" methods. Moreover, specimens subjected to ICR exhibited lower residual capacity. However, data from such experimental studies remain limited. In terms of numerical simulations, Cheng et al. [26] conducted simulations of structures subjected to rigid ICR, demonstrating that the ICR method ignores the impact force, initial damage, and non-zero initial conditions, and underestimates the structural dynamic response. Kang et al. [27] analyzed a three-story steel frame under vehicular impact. The results showed that the overall damage caused by ICR was significantly greater than that of NCR, indicating that the analysis results based on NCR may overestimate the progressive collapse resistance of the structure. Yi et al. [28] simulated the progressive collapse behavior of RC frame structures under ICR at both substructure and structural levels, further confirming that ICR increases collapse risk due to downward pulling forces and initial damage.

The above-mentioned multiple studies have shown that explosion and ICR can cause initial damage to adjacent structural members, reducing their strength and stiffness of structural members. Additionally, extreme loads could generate a downward pulling force at the column removal point (CRP), magnifying the dynamic response of the superstructure, and ultimately resulting in an increased risk of progressive collapse. Therefore, the NCR may not accurately reflect the progressive collapse behavior of building structures when extreme loads are considered. Shi et al. [29] proposed a simplified method that can consider the initial damage of adjacent structural members by applying an initial velocity. The effectiveness and reliability of the proposed method were validated by an example of a three-story, two-span RC spatial frame structure. Further, Shi et al. [30] proposed a substructure-based damage assessment method for RC frame structures, including damage criteria, substructure selection principles, and the calculation of substructure boundary conditions. Li et al. [22] applied the downward pulling force on frame substructures through a drop hammer impact to simulate the downward pulling force generated by explosive column removal.

Mechanics of impact dynamics [31] indicates that the boundary conditions are crucial for the interaction between RC members and superstructures. In crashworthiness studies, the cantilever boundary condition was adopted for some simply-supported bridge piers [32–35], and the axial compressive stress state was considered by applying constant axial loads on the top of frame columns when support displacements were small [36,37]. However, under the scenario of progressive collapse, geometric and material nonlinearities are prominent, so the internal force states of statically indeterminate frame columns will be affected by the change of support displacements. This underscores the need for a more robust approach to modeling boundary conditions in progressive collapse analysis.

Given the limited comprehension about the influence of ICR on the progressive collapse response of RC frame structures, only a few existing research findings concerning impact responses of structural components are applicable to the progressive collapse analysis under ICR. From this perspective, studying the coupling relationship between these two fields could effectively utilize existing experimental results regarding impact and collapse, further expanding the scope of relevant validations and applications. Considering the mechanical principle, this paper studies the interaction between the impact response of frame columns and the progressive collapse response of structures utilizing finite element models (FEMs) established with LS-DYNA. These FEMs were validated by a lateral impact test on RC columns [38] and a static progressive collapse test on RC frame substructures [39], respectively. Considering that the dynamic progressive collapse resistance of structures is related with its static progressive collapse resistance [20,40], the progressive collapse resistance curve of frame beams was used as the boundary condition at the top of columns to analyze the history curve of downward pulling force generated by columns undergoing ICR. Then, the downward pulling force history was input as the external

load of frame beams to obtain their progressive collapse response under ICR. Meanwhile, the response of identical frame beams experiencing direct ICR was simulated and the calculation results of two methods were compared, followed by a discussion about the influence of ICR on the progressive collapse performance of structures.

2. Analysis of impact-collapse coupling framework

Currently, the impact response of concrete columns and the progressive collapse resistance of concrete structures have been comprehensively investigated separately. However, the interaction between impacted columns and superstructures is still unclear. In studies concerning impact resistance, most target objects are single structural columns of which axial compression states are simulated by loading weights. In this condition, actual connections between frame columns and superstructures are not considered, leading to the neglect of their tying effects. On the other hand, progressive collapse studies employing NCR are simple and efficient, but they might overestimate the progressive collapse resistance by ignoring downward pulling force, potentially resulting in unsafe designs. Existing studies [25,28] indicate that when the columns of a frame structure fail due to impact, the pulling effect of column longitudinal bars on the superstructure might increase the risk of progressive collapse (Fig. 1).

ICR may lead to a higher risk of collapse for the following principle: as shown in Fig. 2 (a), for a planar frame structure, the loading method of NCR is equivalent to directly apply an in-plane vertical load F_V to the remaining structure. However, due to the rigid connection of beam-column joints, columns subjected to lateral impact loading F_H could cause a diagonal tensile action N and an out-of-plane torsional action T on superstructures, as shown in Fig. 2 (b). The in-plane vertical downward pulling force N_V of the diagonal tensile action N is the downward pulling force exerted on the superstructure. For the convenience of analysis, this paper adopts an assumption that the in-plane stiffness of the floor slab is infinite. Consequently, the out-of-plane normal degree of freedom (DoF) and the torsional DoF of the mid-column joint are constrained, i.e., the out-of-plane action N_H and the torsional action T are not considered, as shown in Fig. 2 (c). On this basis, a simplified coupling framework is proposed for evaluating the influence of ICR on the progressive collapse resistance of frame structures, as shown in Fig. 3. Firstly, benchmark models were established based on existing tests of a column subjected to impact loading and a frame subjected to NCR. Then, the boundary conditions of benchmark models were transformed. Finally, the coupling relationship between the impact response of columns and the progressive collapse response of structures is established.

2.1. Boundary condition arrangements

The realization of coupling laws relies on boundary condition definitions of column and frame structure models. Firstly, the boundary constraints of the column top are accurately applied to ensure that the deformations at the column top and the superstructure are consistent. The bottom of column model is fixed, as well as all DoFs of the top excepting the vertical translation. The initial load on the structural column and the inertial influence of the superstructure is simulated by attached mass on the column top and global gravitational field. In addition, a nonlinear spring is connected to the column top to simulate the boundary conditions provided by the superstructure, of which stiffness is determined by the collapse resistance of the connected frame beam.

Specifically, a nonlinear static collapse analysis of the frame substructure under NCR is carried out to obtain the static resistance curve $R_s(\mu)$, as shown in Fig. 4. For the RC column model performing impact analysis, its spring stiffness K_{NL} at the column top is defined by Equation (1), which describes the first derivative of the resistance $R_s(\mu)$ with respect to displacements obtained from the quasi-static analysis of the frame substructure to consider the resistance of the superstructure during the impact analysis of column. The maximum elongation Δ_{max} of the spring is determined by Equation (2), i.e., the peak vertical displacement μ_{dmax} of the joint under dynamic NCR analyses of the frame substructure. Given the impact mass and initial velocity, an impact analysis is carried out on the RC column after the boundary transformation. Further, the axial force response history $N_d(t)$ obtained from the impact analysis is extracted as the load input of the frame substructure, which is used to simulate the additional effect of the impact action on the



Fig. 1. Example of collapse caused by column impact failure [41].

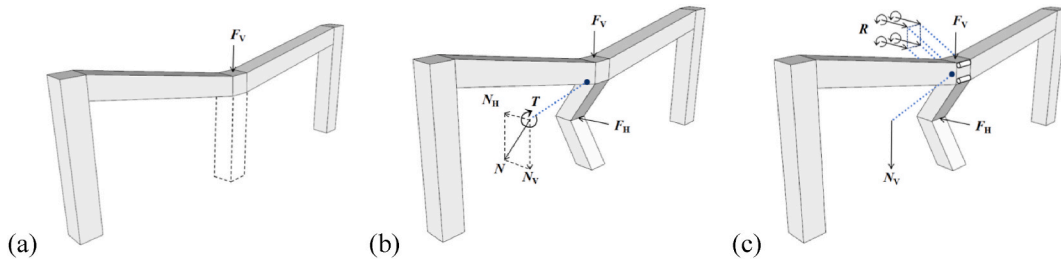


Fig. 2. Three types of column removal conditions. (a) NCR, (b) ICR, (c) ICR with infinite lateral stiffness.

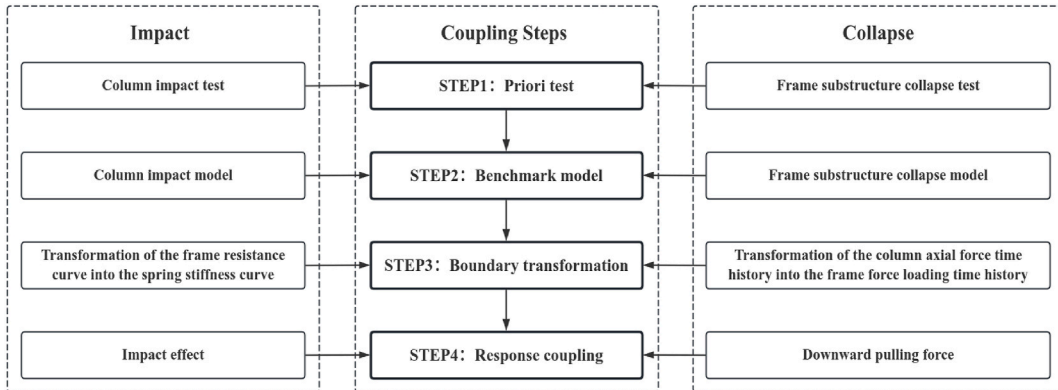


Fig. 3. Coupling flowchart.

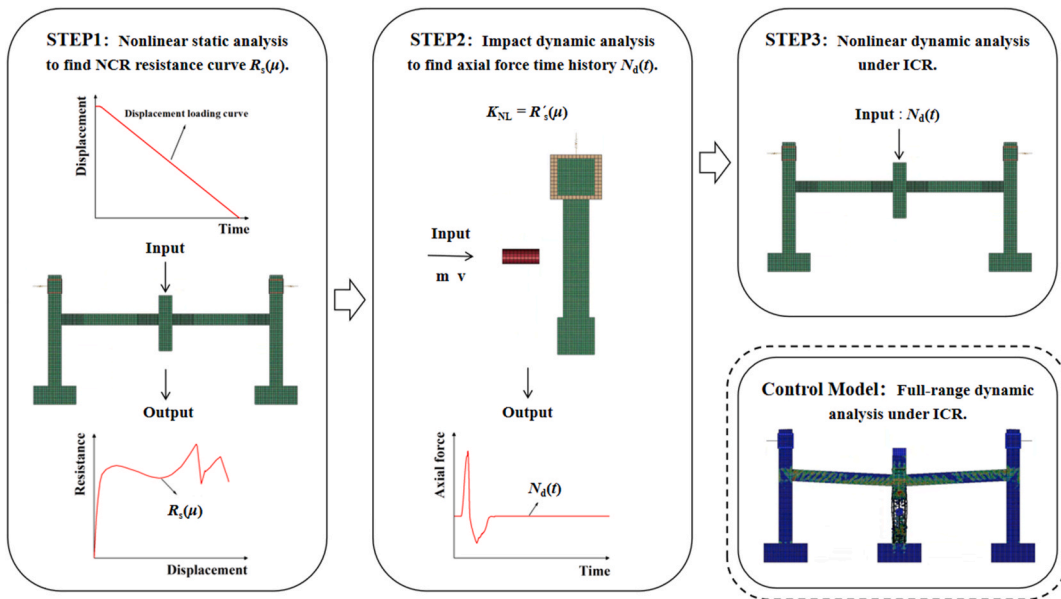


Fig. 4. Coupling boundary settings.

superstructure in the nonlinear dynamic analysis under ICR.

$$K_{NL} = R'_s(\mu) \tag{1}$$

$$\Delta_{max} = \mu_d \max \tag{2}$$

where, NL means nonlinear, μ is vertical displacement of the mid-column joint.

2.2. Validations of the model and analysis method

In this study, the lateral impact test of a RC column and the static NCR test of a RC frame substructure on the mid-column carried out by Zhou et al. [38,39] were selected to validate the accuracy of model parameters and the feasibility of the proposed framework. After preliminary trial calculations and validations, the dynamic load collapse resistance of the frame substructure beam is consistent with that under static load. In addition, Zhou et al. [42] carried out a dynamic NCR test on a substructure with identical dimensions and reinforcement layouts as the static test, and the final failure load of the dynamic specimen was less than the peak resistance of the static specimen. Therefore, for the setting of the spring stiffness at the column top in Section 2.1, the similarity of the structural resistance mechanism under dynamic and static loads and the influence of dynamic effects on the peak resistance need to be comprehensively considered. The accuracy and reliability of the proposed coupling framework are illustrated, on the substructural level, by comparison with the direct ICR analysis. The detailed results are presented in Section 5.

In addition, the coupling framework also indicates an interaction between the impact and the progressive collapse response and further application prospects in event-dependent progressive collapse analyses. Similar simplified analyses can also be carried out in ICR progressive collapse analyses employing different structural forms, element mesh sizes, and materials.

2.3. Approximate dynamic analysis under impact action

Izzuddin et al. [43,44] proposed a structural approximate dynamic analysis method based on the principle of work and energy. This method performs nonlinear static analyses by gradually applying vertical loads on the failed span and upper floors, and then obtaining the static load-displacement curve of structures. Subsequently, the approximate dynamic load-displacement curve of structures is derived according to the law of energy conservation. This method can accurately predict the peak vertical displacement of the failed joint after the sudden removal of load-bearing columns so that the progressive collapse resistance of structures can be readily evaluated. However, this method cannot consider additional dynamic effects caused by ICR, which is investigated in this study by coupling the impact and collapse dynamic response of planar frames based on dynamic FEMs. According to the principle of work and energy, the influence of work done by the downward pulling force and exerted on the superstructure is considered in an approximate dynamic

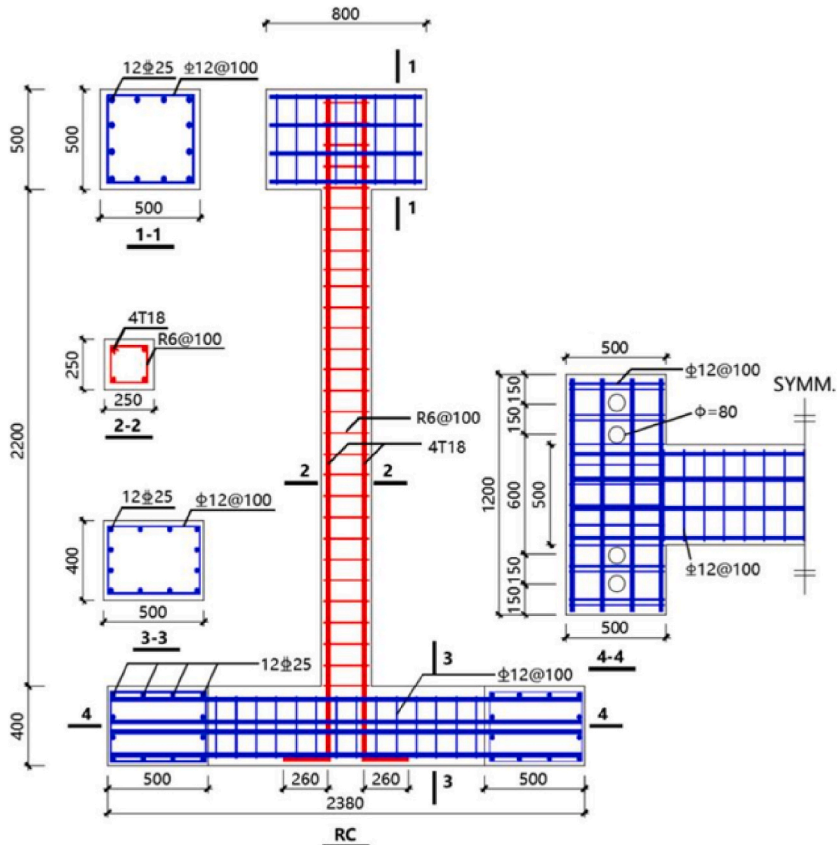


Fig. 5. Dimensions and reinforcement details of specimens (Unit:mm) [38].

analysis method, which is introduced in Section 6.2 for details.

3. Existing tests for validations

3.1. Column impact test

The RC specimen from Ref. [38] was selected as the validation target for impact response. The dimensions and reinforcement details of the specimen are shown in Fig. 5. The compressive strength of concrete cubes was 33.4 MPa, and the mechanical properties of reinforcing bars are presented in Table 1. The pendulum test apparatus is illustrated in Fig. 6. The apparatus takes advantage of the lever principle to apply and magnify the axial load on the top of specimen, and the foundation of specimen is fastened with 8 anchor bolts. The impact was accomplished through the gravitational potential energy of the pendulum. In this study, the selected specimens had an axial compression ratio of 0.39, an impact velocity of 5.8 m/s, and an impact mass of 2.08 t.

3.2. Substructure progressive collapse test

The validation of the frame substructure collapse test adopted from the literature [39], and the specimen size and reinforcement are shown in Fig. 7. The compressive strength of concrete cubes was 27.4 MPa, and the mechanical properties of reinforcing bars are shown in Table 2. As shown in Fig. 8, the test loading device includes four main components: the loading steel frame, the exterior column inflection point restraint device, the mid-column composite restraint device, and the ground beam restraint device. The exterior column inflection point restraint device is used to simulate the actual deformation state of the inflection point of the second-story column, that is, exterior column ends are allowed to rotate within the plane but is restricted from lateral translation. The mid-column composite restraint device enables the mid-column joint to move only vertically and can prevent the in-plane rotation and out-of-plane inclination of the bottom reinforcement of beams on one side of the mid-column joint after fracture. The ground beam restraint device is used to simulate the fixed-end restraint at the bottom of exterior columns. The test applies the axial load through a hydraulic jack on the upper surface of the mid-column. In the initial stage of the test, force-controlled loading is adopted, with an increase of 5 kN per step during the loading stage and a decrease of 3 kN per step during the unloading stage. After the peak strength, displacement-controlled loading is adopted, with an increase of 25 mm per step.

4. Benchmark model

4.1. Modeling process

Tests above were simulated in the numerical software LS-DYNA for model validation. To circumvent the divergence issue, the explicit solution method was utilized to ensure the numerical stability of analyses under large deformation.

4.1.1. Element selection and mesh division

The concrete is modeled by the eight-node solid element (Soild164) with the single-point integration, while the reinforcing bar is modeled by the two-node Hughes-Liu beam element (Beam161) with the 2×2 Gaussian integration. The mesh size of elements is determined according to the mesh sensitivity analysis. The mesh size of concrete elements in the impacted column is 20 mm, and the mesh size of reinforcing bar elements is 10 mm. The mesh size of concrete elements in the frame substructure is 25 mm, and the mesh size at the beam ends is refined to 12.5 mm due to the large deformation. The mesh size of reinforcing bar elements in the frame substructure is 12.5 mm.

4.1.2. Constraint and contact definitions

According to the study conducted by Qian et al. [45], better accuracy can be achieved by separately modeling the reinforcing bar and concrete. So the *CONSTRAINED_BEAM_IN_SOLID keyword is used to define the coupling relationship between beam elements and solid elements employing perfect bond assumptions. The *CONTACT_AUTOMATIC_SURFACE_TO_SURFACE is used to simulate the contact relationship between the specimen and the hammer head, the specimen and the loading mass block, and the specimen and the rigid body restraint.

4.1.3. Boundary conditions and loading method

The *BOUNDARY_SPC_SET keyword is used to constrain all DoFs of nodes at the bottom of the column and the spring end. When conducting the column impact analysis, the axial compression of the model is achieved by applying gravity to the loading weight using the *LOAD_BODY_Y keyword, and the impact load is achieved by applying an initial velocity to the pendulum using the

Table 1
Material properties of reinforcing bars.

Type/(mm)	Yield Strength/(MPa)	Ultimate Strength/(MPa)	Elongation Rate/(%)
R6	455.70	674.70	33.7
T18	442.30	624.00	26.0

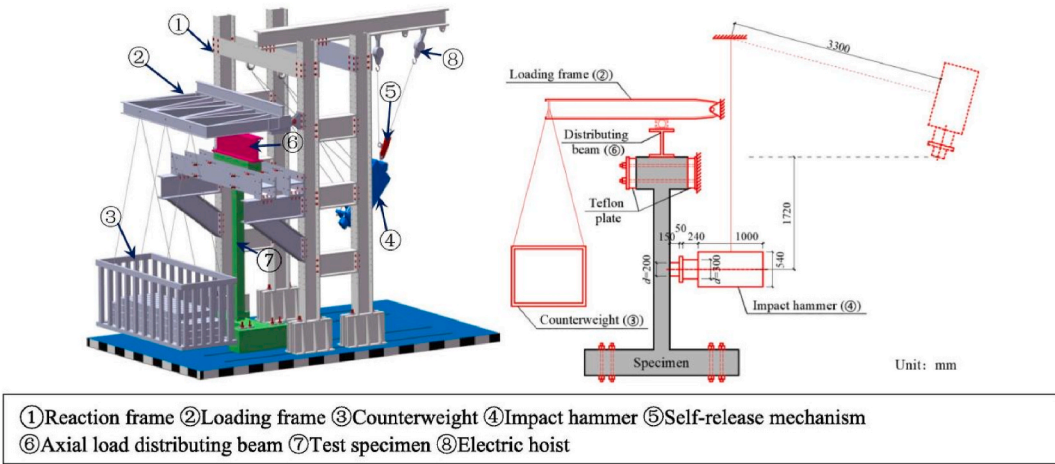


Fig. 6. Test setup and loading schemes [38].

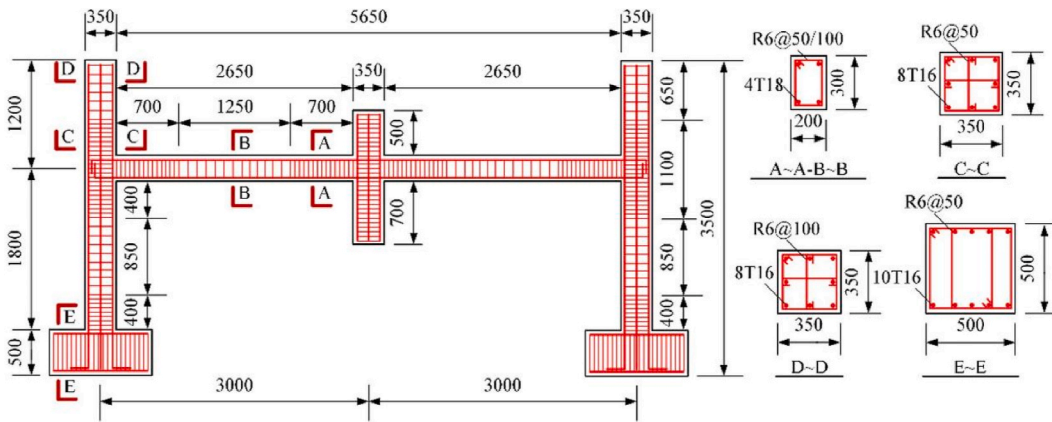


Fig. 7. Dimensions and cross sectional details of test specimen(Unit:mm) [39].

Table 2

Material properties of reinforcing bars.

Type/(mm)	Yield Strength/(MPa)	Ultimate Strength/(MPa)	Elongation Rate/(%)
R6	385	460	26.0
T16	505	630	28.0
T18	485	622	24.0

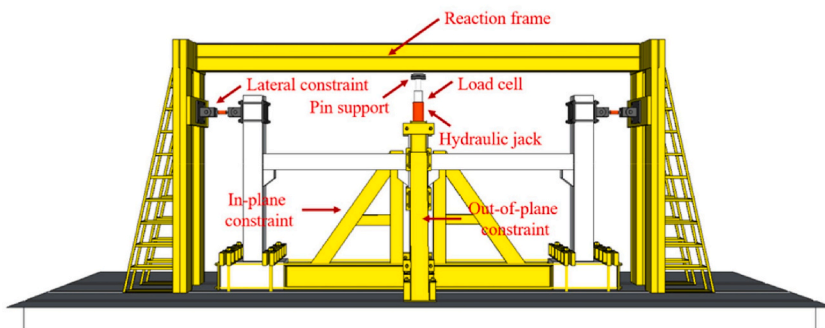


Fig. 8. Test setup and loading method [39].

*INITIAL_VELOCITY keyword. When conducting the static analysis of the frame substructure, displacement-controlled loading is adopted using the *BOUNDARY_PRESCRIBED_MOTION_SET keyword, and force-controlled loading is applied on the mid-column utilizing the *RIGID_BODY_FORCE_NODE keyword when performing direct ICR analysis of the frame substructure.

4.2. Material constitutive relationship

4.2.1. Concrete

The concrete adopts the Continuous Surface Cap Model (CSCM), in which the failure surface is jointly defined by three stress invariants and a cap hardening parameter [46]. The CSCM can set element erosion according to the maximum principal strain. However, when this criterion is solely used for erosion, it has limitations in simulating shear failures. Given that the test substructure has obvious shear deformation, the erosion criterion *MAT_ADD_EROSION is used to define the maximum shear strain of the concrete (0.3 is taken in this paper). It should be noted that element erosion is not an actual physical phenomenon in material behavior, but a computational tool used to solve the distortion of the Lagrangian mesh under large deformation [47]. And in the CSCM, IRATE = 1 was chosen to activate the inbuilt strain-rate effect algorithm, which could lead to an increase in material strength in concrete elements when the strain rate is considerable.

The CSCM model can be parameterized in two ways, namely *MAT_CSCM_CONCRET with simple input and *MAT_CSCM with full parameter input. When using simple input, only the unconfined compressive strength, the maximum aggregate size, and the unit system are required. However, it is found in the simulation that the simple input will overpredict the actual resistance of structures. Therefore, the full parameter input is adopted in this paper. Nevertheless, a literature [48] shows that automatically generated parameters of the CSCM with full parameter input also overpredict the structural stiffness. According to suggestions from the model developers, the tensile fracture energy G_{ft} is reduced to 80 % of the default value. When the compression damage and shear damage are obvious, the compression fracture energy G_{fc} and the shear fracture energy G_{fs} are respectively calibrated to $50G_{ft}$ and $0.5G_{ft}$ [49,50], and the remaining parameters are calculated according to the material user manual [49].

4.2.2. Reinforcing bars

The constitutive model of reinforcing bars selects the *MAT_PLASTIC_KINEMATIC. This model can adjust the material characteristics of the model through the hardening parameter β . When $\beta = 0$, it is a kinematic hardening model; when $\beta = 1$, it is an isotropic hardening model; when β is between 0 and 1, it is a combined hardening model. Since the mechanical properties of the reinforcing bar in tension and compression are similar, isotropic hardening is preferred, so the β value is set to 1. The Cowper-Symonds model was

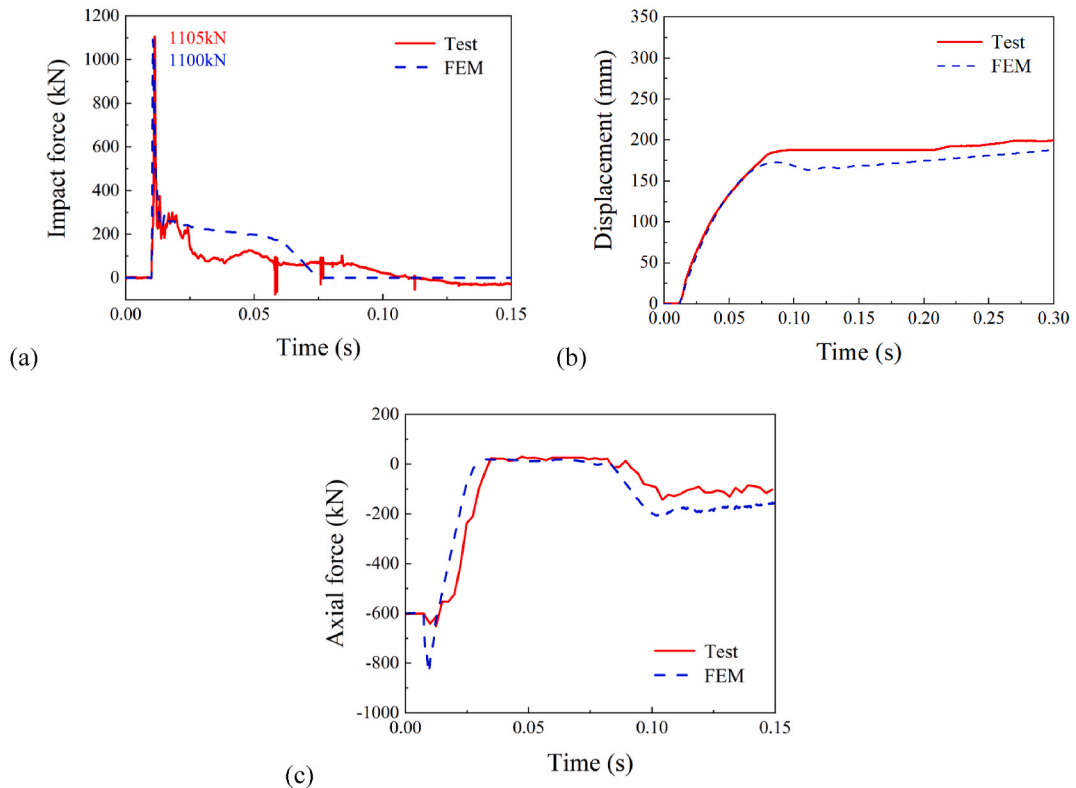


Fig. 9. Comparison of experimental and FE model results. (a) Impact force; (b) Displacement; (c) Axial force.

employed to simulate the strain rate effects of the rebar in this material model, with strain rate parameters C and P defined as 40.4 s^{-1} and 5 [47]. In addition, in the Plastic Kinematic model, beam elements will be deleted when the strain exceeds the preset ultimate strain value. In this study, the maximum ultimate strain of beam elements representing reinforcing bars is based on the elongation rate obtained from material property tests.

4.2.3. Other material models

In addition to the concrete and reinforcing bar material models, the exterior column restraint and mid-column loading of the frame substructure, as well as the loading weight and restraint of the column, all adopt the rigid body material model *MAT_RIGID. The elastic modulus and Poisson’s ratio adopt the parameters of steel, and the density is converted according to the experimental values. The exterior column restraint device in the experiment did not undergo obvious plastic deformation, so the exterior column restraint in the model adopts an elastic boundary. In addition, in order to consider the influence of the boundary restraint stiffness, discrete spring elements using the linear elastic spring material model *MAT_SPRING_ELASTIC are set at the inflection point of the exterior column of the frame substructure, and the spring stiffness is taken as 9.1 kN/mm according to experimental data. The equivalent spring of the frame beam at the column top adopts the nonlinear spring material model *MAT_NONLINIER_ELASTIC, in which the spring stiffness curve is taken as the first derivative of the quasi-static resistance curve with respect to displacements of the frame substructure.

4.3. Model validations

4.3.1. Validation of column impact test

Fig. 9(a) exhibits the comparison of impact force history curves between the experimental and numerical results, which is in good agreement in terms of overall development trends. The impact force history curve can be conceptually classified into three stages: the peak stage, the stable stage, and the attenuation stage. The peak stage obtained by numerical calculation is maintained at about 2.5 ms, the impact force duration is about 70 ms, and the peak impact force is 1100 kN, which is slightly smaller than the test results. The error compared with the test value is within 5 %, indicating a relatively high accuracy.

Fig. 9 (b) compares horizontal displacement history curves at the impact point of columns between experimental and numerical results. It can also be classified into three stages: the loading stage, the unloading stage, and the axial compression stage. Good agreements between the FE model and the experimental data can be observed in the early loading stage. Admittedly, there is a certain difference between the displacement peak value of the FE model and the experimental result, which could be ascribed to various factors, such as the simplified assumptions of the FE model, the approximate methods used in the calculation process, the incomplete control of the experimental conditions, etc. In addition, the concrete near the impact point in the specimen column undergoes severe punching shear failure. However, the FE model deletes the elements exceeding the maximum principal strain or shear strain based on the erosion algorithm, which struggles to accurately simulate cracking and subsequent concrete fractures. These factors result in above-mentioned differences between FE model and experimental results.

Fig. 9 (c) compares axial force history curves between experimental and numerical results. It can be observed that the overall trend of the FEM curve is in good agreement with the experimental results. The initial axial force is approximately 600 kN. When the impact head collides with the column surface, the axial force of the specimen increases rapidly within a short period. After reaching the peak axial force, the impact causes a loss of vertical load-bearing capacity, leading to a decrease in the axial force until it drops to zero. Subsequently, due to the falling of the loading frame, the axial force increases again. However, because the column stiffness is reduced due to damage, the axial force is smaller than the initial value. The simulated peak axial force and residual axial force are greater than the experimental values, which may be attributed to the fact that the reaction frame in the experiment is not perfectly rigid, whereas the axial compression distribution beam in the FEM is modeled as a rigid body material.

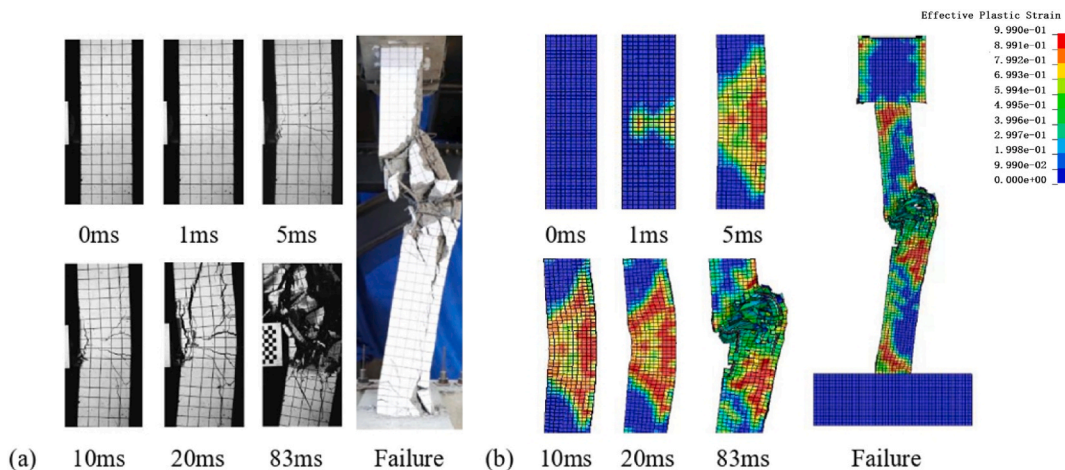


Fig. 10. Damage comparison. (a) RC specimen from the test; (b) FE model.

Fig. 10 compares the damage patterns of the test and the FE model at 0 ms, 1 ms, 5 ms, 10 ms, 20 ms, and 83 ms. The comparison indicates that the model can reasonably predict the damage evolution and failure mode of the column. The final failure pattern is the shear failure with crushed concrete around the impact point. The overall failure process of FE model is basically consistent with the test. So the impact-collapse coupling model developed using this FE model promises a certain degree of accuracy.

4.3.2. Validation of frame substructure collapse test

Fig. 11 (a) compares the static load-displacement curves between the test and FE model, which develops in similar trends. Progressive collapse responses of the substructure are divided into the beam action, the compressive arch action (CAA), and the catenary action (CA). Differences between the test and FE model on demarcation and peak points at each stage are all within 10 % (see Table 3).

Fig. 11(b) shows the comparison of lateral displacement curves of the exterior beam-column joints. Despite relative high consistency in the overall trends, the outward displacement in the CAA stage and the inward displacement in the CA stage of the FE model curve are both smaller than the test results. This might be owing to the relatively rigid boundary conditions and material properties in the FE model compared to the test.

Fig. 12 compares the damage patterns of the test and the FE model. It is shown that the FE model accurately reflects the failure characteristics of the tested specimen. In the initial stage of loading, a few flexural cracks formed on the frame beam. With the increase of loads, the CAA was identified because the lower part of the mid-column joint area of the frame beam and the upper part of the exterior column joint are in tension, as well as the arched compressive zone. As the displacement of the mid-column joint increases, the cracks in the concrete tensile zone develop, and the compressive zone is crushed. The strains of the upper and lower reinforcing bars in the mid-span of the frame beam change from compression to tension. The CA develops until the reinforcing bars at the mid-column beam end and the exterior column beam end fractured, ultimately leading to structure failure. It can be seen that this model has high accuracy and can be used as a benchmark model for subsequent impact-collapse analysis.

5. Implementation of impact-collapse coupling framework

This section demonstrates the computational effectiveness and efficiency of the proposed impact-collapse coupling framework utilizing the frame substructure model validated in section 4.3.2. The column of the substructure model was extracted and separately modeled, which was used to evaluate the effectiveness of the proposed framework. Then, results from the coupling model and the direct ICR model were further compared. The calculation time spent on the direct ICR model is approximately 5 h, while the coupling model took only around 3 h, exhibiting apparent computational efficiency.

5.1. CRP displacement between column and substructure models

The extraction of the column model follows the methodology setting the coupling boundary that described in Fig. 4. Then, the top vertical displacement history of the extracted column model and the frame substructure model practicing the coupling framework are compared in Fig. 13, in which the red line represents the extracted column model and the blue dashed line represents the coupling model. Both curves exhibit almost identical trends, indicating that the simplified boundary and loading methods are properly applied and can accurately capture the interaction and force transfer between the impacted column and superstructure.

5.2. Comparisons between the coupling model and direct ICR model

Fig. 14 compares the structural damage development of the coupling model and the direct ICR model. According to the findings from Yi et al. [28], the progressive collapse process of ICR can be divided into the impact loading stage and the gravity loading stage, and Fig. 15 (a) indicates that the critical point of the two stages is approximately 120 ms. During the impact loading stage, local punching shear failures first occurred near the impact point when the impact began. Simultaneously, the shock wave propagated in the column, producing an instantaneous upward impact on the CRP. With further development of the lateral displacement on the impact point, column reinforcing bars begin to exert the downward pulling force on the superstructure, as signified by the CRP acceleration exceeding gravitational acceleration and rapid increases in CRP vertical displacement. Subsequently, the concrete elements near the impact point completely failed, with the reinforcing bar fracturing, and the structure entered the gravity loading stage. In this stage, the development of structural resistance is similar to those employing NCR.

Fig. 15 (a) compares the axial force history transmitted from the column to the beam in the coupling model and the direct ICR models, respectively. In the coupling model, the force is obtained through the contact force with the column, while in the direct ICR model, it is obtained through the sectional force. The curves first experience the upward pulse effect on the beam in the impact arching stage, and then changes to the downward pulling force. Finally, the column was removed due to complete fractures of column

Table 3
Comparison of the force conditions between experiment and FE results.

Category	CAA Peak/(kN)	Demarcation point/(kN)	CA Peak/(kN)
Test	119.2	109.7	145.3
FEM	119.6	103.3	147.2
Deviation	+0.3 %	-5.8 %	+1.3 %

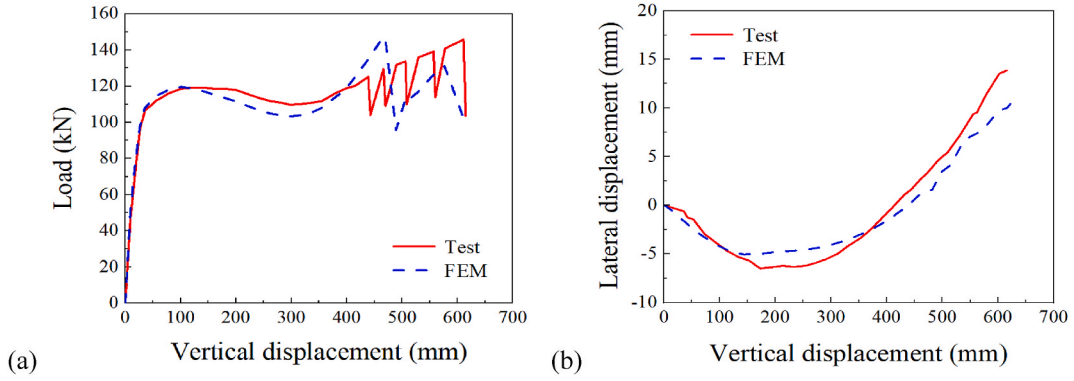


Fig. 11. Comparison of experimental and FE results. (a) Load-displacement; (b) Lateral displacement.

reinforcing bars. The peak errors in the arching stage and the downward pulling stage are both less than 10%. Fig. 15(b) compares the vertical displacement history at the beam-column joint of the two models. Clearly, displacement trends of the two models are highly consistent, and the errors at each moment are kept within 5%, further illustrating the accuracy and reliability of the proposed coupling framework.

6. The progressive collapse resistance of frame structures under ICR

6.1. Downward pulling force

As shown in Fig. 15 (a), when using the ICR, the beam-column joint was initially subjected to an upward force. Then the force direction changed due to the development of the impact process and the structural response. A portion of the load originally supported by the column is redistributed to adjacent structural components, such as beams, resulting in a downward pulling force at the beam-column joint. Compared with the NCR, the downward pulling force obviously increased the vertical load of the structure, resulting in higher collapse risks under the combined action of gravity loads and downward pulling force.

In order to compare the influence of ICR and NCR on the collapse performance of the structure, on the basis of the ICR model, the simulation of NCR was realized by defining the failure time with *MAT_ADD_EROSION. Fig. 16 shows the displacement history of the joints in the structure and the final damage state under the two working conditions with identical additional masses. As shown in the figure, the peak vertical displacement of the CRP in the NCR model is 26 mm, and the peak vertical displacement of the CRP in the ICR is 110 mm. The displacement of the CRP in the structure is significantly increased under the ICR condition due to the downward pulling force. Therefore, ignoring the influence of impact on the progressive collapse of structures might underestimate the structural load, leading to unsafe structural design.

6.2. Discussion based on the energy balance method

As shown in Fig. 17, according to the Energy Balance Method (EBM) proposed by Izzuddin et al. [43,44], it is assumed that mechanical principles and failure modes of structures under dynamic conditions are the same as those under static conditions. Therefore, the work done by the additional gravity load W_{p_d} is equal to the sum of the kinetic energy E_K and strain energy of the structure U during the progressive collapse of structures. Accordingly, W_{p_d} is the product of the additional gravity load P_d and the peak vertical displacement of the middle joint μ_d . U can be obtained by numerically integrating the vertical resistance $P(\mu)$ obtained from the static analysis of the structure with respect to the vertical displacement of the middle joint μ , which can be respectively expressed as Equation (3) and Equation (4). If the progressive collapse of the structure is to be prevented at a certain deflection, the velocity of the structure needs to be reduced to zero. At this time, $E_K = 0$, and W_{p_d} should be equal to the U absorbed by the structure, which is expressed in Equation (5). It should be noted that the energy method ignores the influence of strain rate and damping. Cheng et al. [47] compared with the results of incremental dynamic analysis, indicating that EBM, as a simplified evaluation method, can accurately evaluate the dynamic resistance of the structure without considering the influence of strain rate and damping ratio.

$$W_{p_d} = P_d \cdot \mu_d \quad (3)$$

$$U = \int_0^{\mu_d} P(\mu) d\mu \quad (4)$$

$$P_d \cdot \mu_d = \int_0^{\mu_d} P(\mu) d\mu \quad (5)$$

However, for ICR, when extra vertical displacements generate at the CRP under the impact load, both the downward pulling force

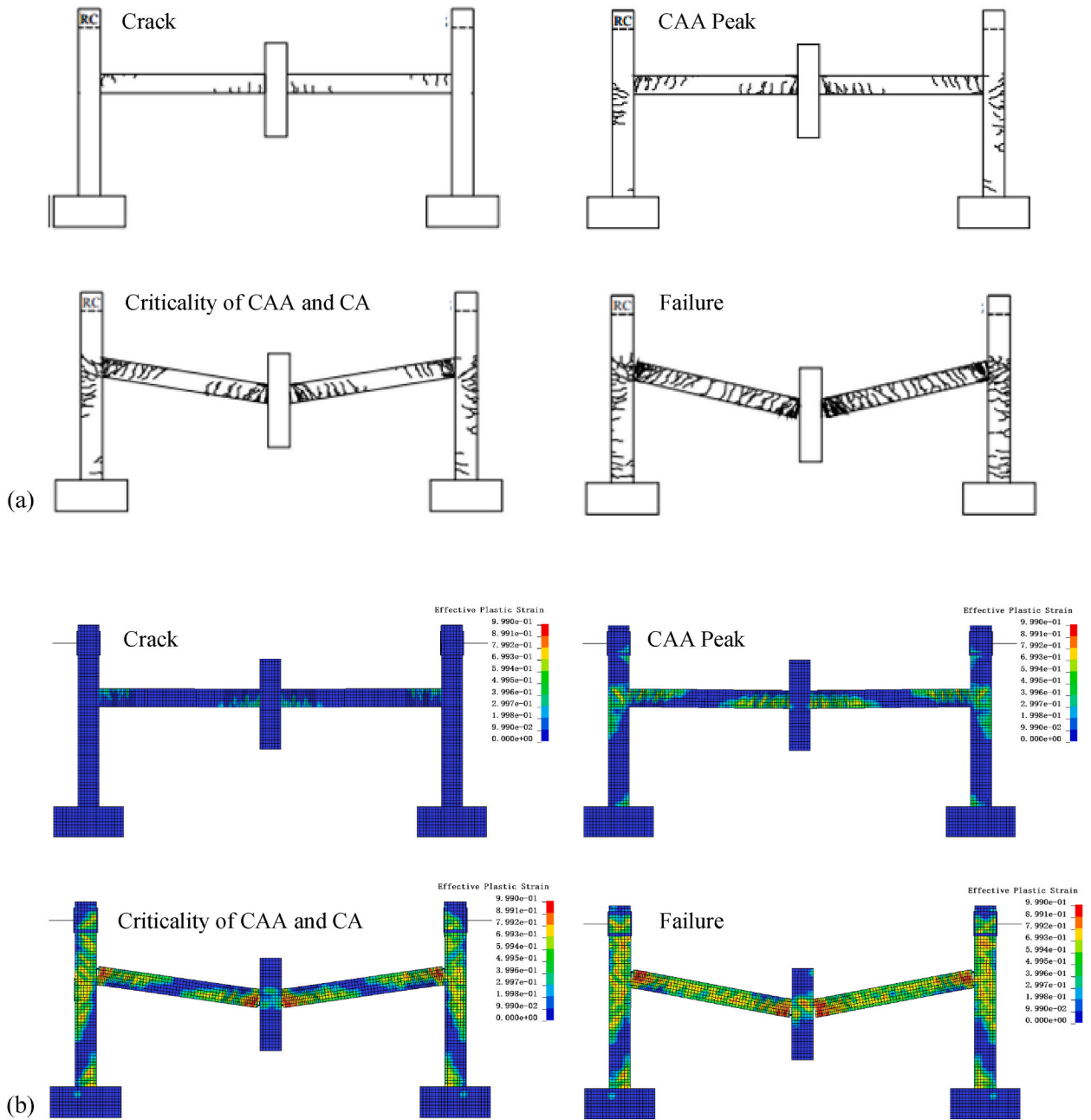


Fig. 12. Damage comparison. (a) RC specimen from the test; (b) FE model.

of the failed column and the additional gravity load generate external work. The work done by the downward pulling force W_N could be obtained by integrating the axial force N with respect to the vertical displacement of the middle joint μ , which is expressed as Equation (6). At this time, according to the conservation of mechanical energy, the sum of W_N and W_{P_d} is equal to the structural strain energy U , as shown in Equation (7).

$$W_N = \int_0^{\mu_d} N(\mu) d\mu \tag{6}$$

$$\int_0^{\mu_d} N(\mu) d\mu + P_d \cdot \mu_d = \int_0^{\mu_d} P(\mu) d\mu \tag{7}$$

From the energy perspective, due to the additional external work done by the downward pulling force, more structural strain

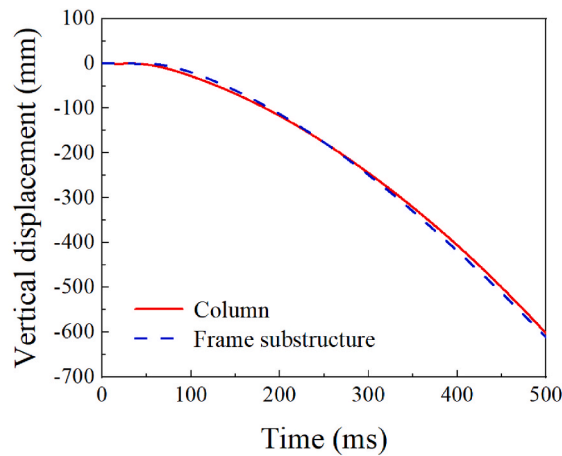


Fig. 13. Displacement history of the mid-column joint

potential energy is required to dissipate the external work. Therefore, the displacement of CRP further develops, increasing the risk of progressive collapse of the structure.

6.3. Influence of impact velocity and mass

The aforementioned comparative analysis shows that the impact loading yields significant influence on the collapse performance of structures, which is ascribed to the downward pulling force exerted by the failed column on the superstructure. On the other hand, the impact effects are mainly influenced by the impact velocity and the impact mass. Therefore, further investigations on six models with different velocity-mass combinations, as listed in Table 4, are performed in this section to discuss factors influencing the downward pulling force and corresponding performance of structures.

As shown in Fig. 18, when the impact mass is kept constant and the impact velocity increases from 15 m/s to 20 m/s, the action time of the column downward pulling force at the joint is shortened while the peak value is reduced. When the impact velocity is kept constant and the impact mass is taken as m , $2m$, and $3m$, respectively, the action time of the column downward pulling force at the joint is shortened with the increase of the impact mass, and this phenomenon is more obvious when the impact mass is small. It is worth mentioning that the change of impact mass has almost no effect on the peak value of the downward pulling force. In addition, compared to the impact mass, the impact velocity has a more significant effect on the action time of the column downward pulling force. Furthermore, the impact mass has a minor effect on the downward pulling force, with impact velocity being the main influencing factor. Moreover, it is obvious that the time taken by columns to fail increases as the impact velocity decreases, resulting in a longer impact loading stage. Consequently, the downward pulling force would lead to more unfavorable effects on the progressive collapse resistance of superstructures.

6.4. Influence of longitudinal reinforcement strength and reinforcement ratio

The downward pulling force transmitted by the impacted column to the superstructure is provided by the longitudinal reinforcement of the column. The peak downward pulling force should be related to the reinforcement ratio and strength of the longitudinal reinforcement. Therefore, this section conducts a numerical study on the impact-induced progressive collapse of RC frame substructures with different longitudinal reinforcement strengths and reinforcement ratios under the same impact loading conditions.

The parameters of longitudinal reinforcement with different strength grades are shown in Table 5. As shown in Fig. 19, as the strength grade of the longitudinal reinforcement increases, the downward pulling force exerted by the impacted column on the remaining superstructure increases. When the strength grade of the longitudinal reinforcement is increased from HPB300 to HRB335, HRB400, and HRB500, the peak values of the downward pulling force increase from 145 kN to 233 kN, 399 kN, and 582 kN respectively.

Fig. 20 shows the time-history curves of the downward pulling force of the RC frame substructure when the unilateral reinforcement ratios under impact-induced column loss are 1.01 %, 1.31 %, 1.66 % and 2.05 % respectively. Here, the reinforcement ratio is modified by changing the diameter of the longitudinal reinforcement, and the corresponding values of the longitudinal reinforcement diameter are 14 mm, 16 mm, 18 mm and 20 mm respectively. It can be seen from the figure that as the longitudinal reinforcement ratio increases, the downward pulling force exerted by the impacted column on the remaining superstructure increases. When the longitudinal reinforcement ratio increases from 1.01 % to 1.31 %, 1.66 % and 2.05 %, the peak values of the downward pulling force increase from 233 kN to 532 kN, 746 kN and 933 kN respectively.

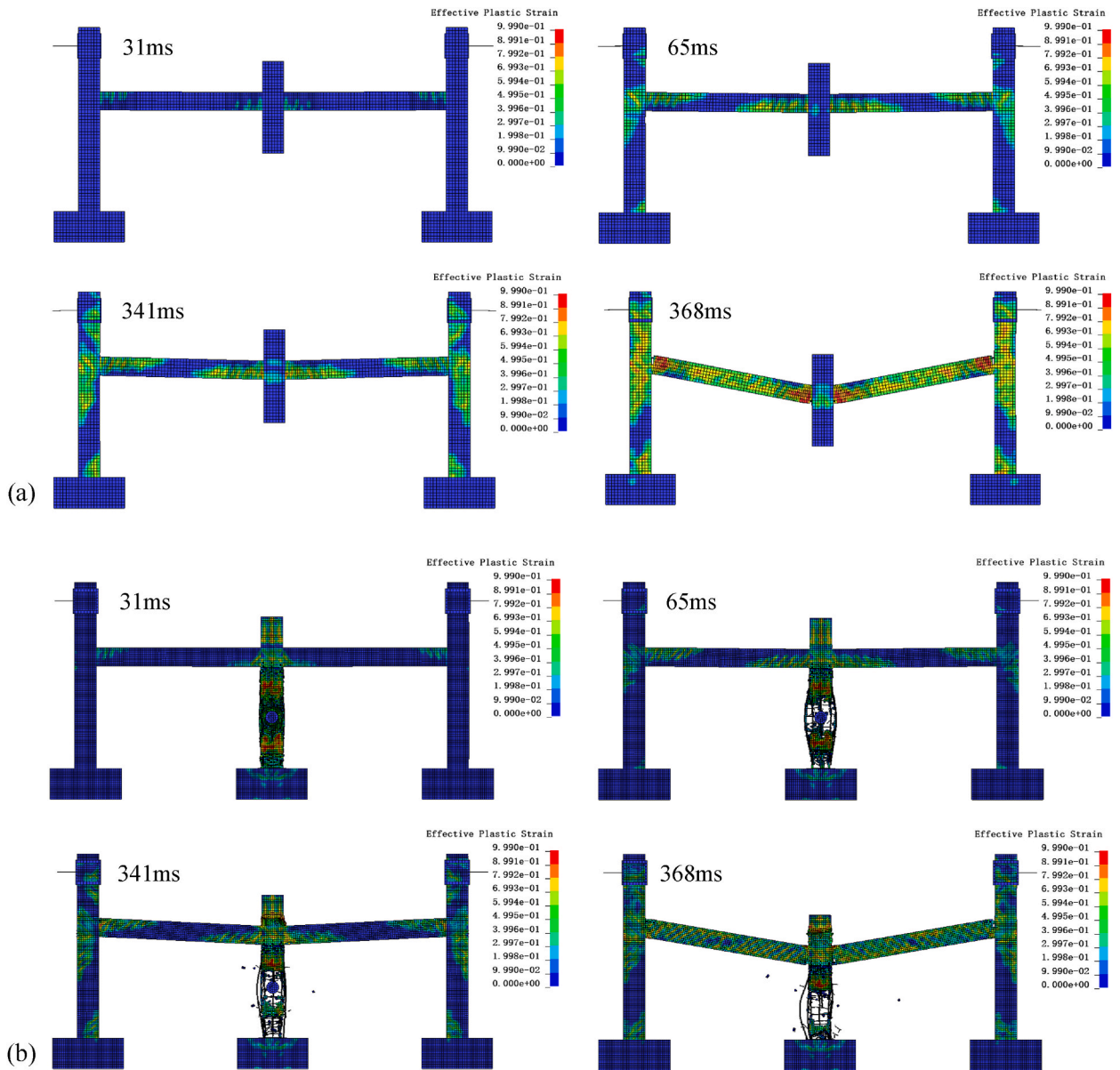


Fig. 14. Damage comparison. (a) coupling model; (b) direct ICR model

7. Conclusions

Inspired by recent event-dependent progressive collapse studies, an analytical framework coupling the impact response of RC columns with the progressive collapse performance of RC frame substructures is proposed in this study. This framework offers improvements over traditional approaches based on NCR. While NCR does not account for the dynamic effects of impact, the proposed framework incorporates the downward pulling force exerted by impacted columns on the superstructure, which may provide a more realistic understanding of collapse risk. By considering dynamic interactions between impacted columns and the superstructure, the framework shows potential for enhanced accuracy in predicting structural behavior under extreme loading conditions, such as those caused by vehicle collisions or blast events. Moreover, the framework decoupling the impact and collapse analyses allows for the use of existing experimental data for validation and calibration. While in this study, the subsequent validations and applications, performed in the LS-DYNA environment, are presented through models of RC columns subjected to impact loading and RC frame substructures underwent column removal, respectively. The progressive collapse of RC frame structures under impact-induced column removal was studied by analyzing the influence of downward pulling force. The main conclusions are as follows:

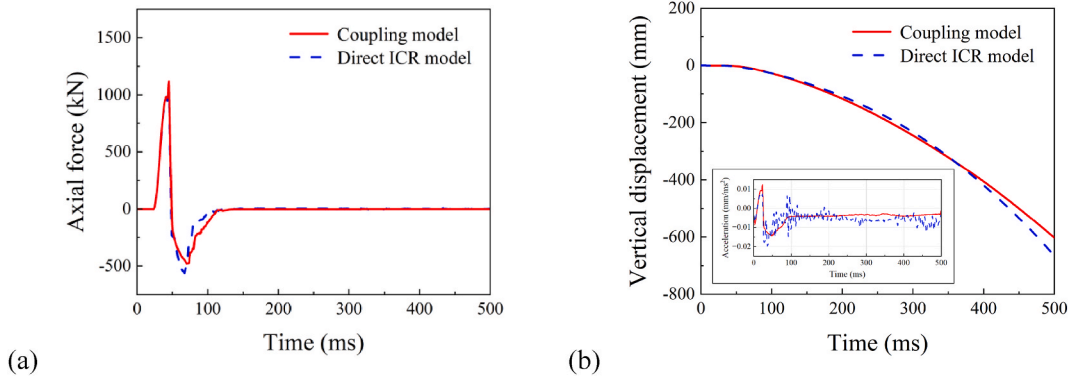


Fig. 15. Comparison of results between two substructural models. (a) Axial force; (b) Displacement.

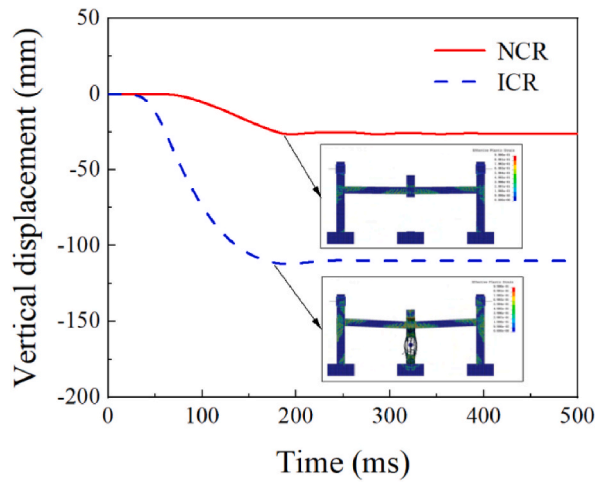


Fig. 16. Comparison of vertical displacement history at the middle beam-column joint.

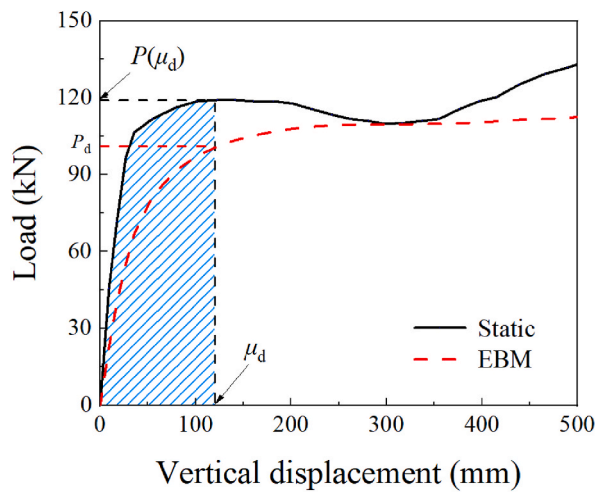


Fig. 17. Illustration of energy balance method.

Table 4
Parameters of models with varied velocity and mass.

Working conditions	Impact velocity	Impact mass
1	15 m/s	m
2	15 m/s	2m
3	15 m/s	3m
4	20 m/s	m
5	20 m/s	2m
6	20 m/s	3m

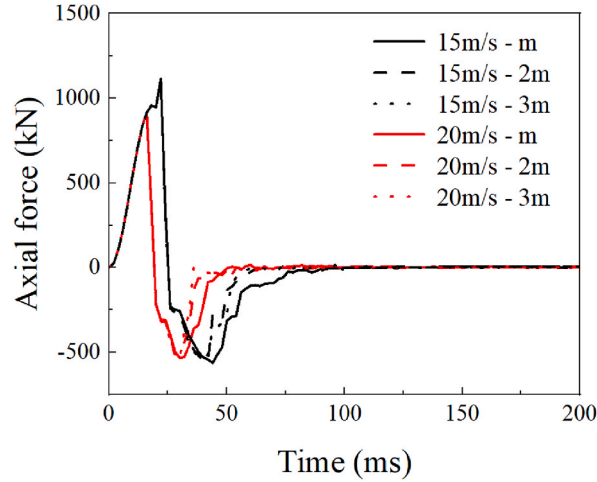


Fig. 18. Axial force history with different velocities and masses.

Table 5
Parameters of longitudinal reinforcement with different strength grades.

Strength Grade	Yield Strength/(MPa)	Ultimate Strength/(MPa)
HPB300	329	470
HRB335	368	525
HRB400	432	618
HRB500	549	784

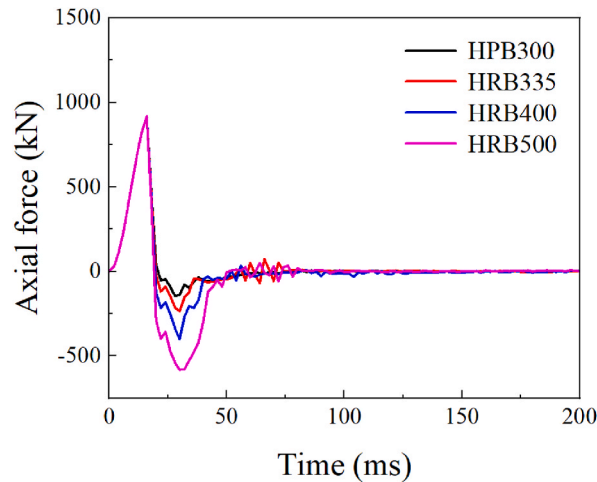


Fig. 19. Axial force - history with different longitudinal reinforcement strength.

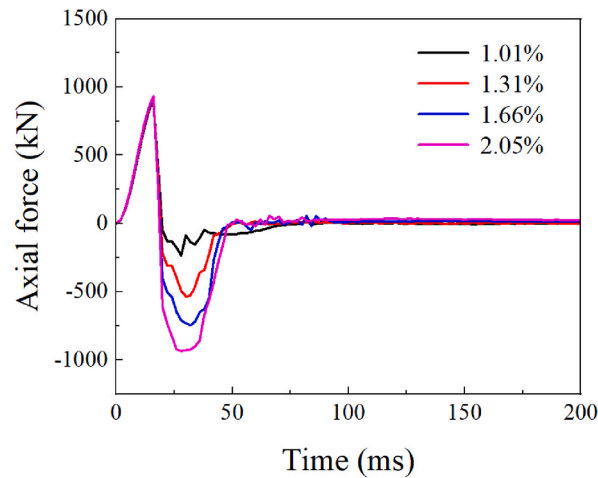


Fig. 20. Axial force - history with different reinforcement ratios.

- (1) Models validating the impact response of RC columns and progressive collapse performance of RC frame substructures exhibited good consistency with the test results in terms of impact force history curves, collapse resistance curves, damage modes, etc., offering reliable benchmark models for the subsequent coupling analysis of impact and collapse responses.
- (2) An impact-collapse coupling framework was proposed, in which the progressive collapse resistance of frame substructures is treated as the restraint stiffness curve at the top of frame columns. Then, the spring boundary force history curve at the column top was extracted and input as the load of the frame substructure benchmark model for analyzing the influence of ICR on the progressive collapse resistance of structures. While ensuring the accuracy of calculations, compared with the direct ICR model, the coupling analysis is more promising because of its higher computational efficiency and potential of combining test data of impact and progressive collapse response.
- (3) The impact loading yields a downward pulling force on the superstructure and increases the progressive collapse risk of structures. Compared with the NCR, the downward pulling force increases the vertical load of the structure. From the energy perspective, due to the additional external work done by the downward pulling force, more structural strain potential energy is required for dissipating the external work, resulting in a larger displacement at the CRP and a higher collapse risk. Therefore, the influence of downward pulling force needs to be considered when analyzing progressive collapse resistance of structures subjected to ICR.
- (4) The influence of impact velocity, impact mass, longitudinal reinforcement strength and reinforcement ratio on the progressive collapse resistance of the structure is discussed and evaluated. The analysis shows that, compared with the impact mass, the impact velocity has more significant influence on the duration of the downward pulling force. With the decrease of impact velocity, the duration of columns exerting downward pulling force would increase. Higher reinforcement strength or reinforcement ratios also lead to a larger downward pulling force, resulting in more unfavorable effects on the progressive collapse resistance of superstructures.

CRediT authorship contribution statement

Yun Zhou: Writing – review & editing, Methodology, Funding acquisition, Conceptualization. **Ting Li:** Writing – original draft, Validation, Formal analysis. **Fan Yi:** Writing – review & editing, Methodology. **Fei-Fan Feng:** Visualization. **Jing-Ming Sun:** Software. **Wei-Jian Yi:** Supervision, Conceptualization.

Declaration of competing interest

The authors declare that there is no conflict of interest regarding the publication of this paper.

Acknowledgements

The authors sincerely appreciate the funding support provided by the National Natural Science Foundation of China (NSFC) (No.52278306), the Key Research and Development Program of Hunan Province (No. 2022SK2096), the Hunan Provincial Natural Science Foundation of China (No. 2023JJ70003), the National Natural Science Foundation of China (No. 52408327), the Natural Science Foundation of Hunan Province, China (No. 2024JJ6198).

Data availability

Data will be made available on request.

References

- [1] American Society of Civil Engineers (ASCE), *Minimum Design Loads and Associated Criteria for Buildings and Other Structures*, ASCE, Reston, Virginia, USA, 2022.
- [2] C. Pearson, N. Delatte, Ronan point apartment tower collapse and its effect on building codes, *J. Perform. Constr. Facil.* 19 (2) (2005) 172–177, [https://doi.org/10.1061/\(ASCE\)0887-3828\(2005\)19:2\(172\)](https://doi.org/10.1061/(ASCE)0887-3828(2005)19:2(172)).
- [3] B. Pfefferbaum, Lessons from the 1995 bombing of the Alfred P. Murrah federal building in Oklahoma city, *Lancet* 358 (9286) (2001) 940, [https://doi.org/10.1016/S0140-6736\(01\)06118-9](https://doi.org/10.1016/S0140-6736(01)06118-9).
- [4] Z.P. Bazant, M. Verdure, Mechanics of progressive collapse: learning from World Trade Center and building demolitions, *J. Eng. Mech.* 133 (3) (2007) 308–319, [https://doi.org/10.1061/\(ASCE\)0733-9399\(2007\)133:3\(308\)](https://doi.org/10.1061/(ASCE)0733-9399(2007)133:3(308)).
- [5] Department of Defense (DOD), *Design of Buildings to Resist Progressive Collapse*, DOD, Washington DC, USA, 2016.
- [6] United States General Services Administration (GSA), *Progressive Collapse Analysis and Design Guidelines for New Federal Office Buildings and Major Modernization Projects*, GSA, Washington DC, USA, 2016.
- [7] China Association for Engineering Construction Standardization (CECS), *Code for Anti-collapse Design of Building Structures*, CECS, Beijing, China, 2021 (in Chinese).
- [8] W. Yi, Q. He, Y. Xiao, Collapse performance of RC frame structure, *J. Build. Struct.* 5 (2007) 104–109+117, <https://doi.org/10.14006/j.jzjgxb.2007.05.013> (in Chinese).
- [9] K. Qian, B. Li, Experimental and analytical assessment on RC interior beam-column subassemblages for progressive collapse, *J. Perform. Constr. Facil.* 26 (5) (2012) 576–589, [https://doi.org/10.1061/\(ASCE\)CF.1943-5509.0000284](https://doi.org/10.1061/(ASCE)CF.1943-5509.0000284).
- [10] A.T. Pham, K.H. Tan, Experimental study on dynamic responses of reinforced concrete frames under sudden column removal applying concentrated loading, *Eng. Struct.* 139 (2017) 31–45, <https://doi.org/10.1016/j.engstruct.2017.02.002>.
- [11] K. Qian, X.-Y. Chen, T. Huang, Dynamic response of RC beam-slab substructures following instantaneous removal of columns, *J. Build. Eng.* 45 (2022) 103554, <https://doi.org/10.1016/j.job.2021.103554>.
- [12] X.-J. Yang, F. Lin, X.-L. Gu, Progressive collapse resistance of RC beam-slab substructure under two-adjacent-edge-columns removal scenario, *J. Build. Eng.* 80 (2023) 108115, <https://doi.org/10.1016/j.job.2023.108115>.
- [13] N. Makood, A. Setiawan, M. Buitrago, J.M. Adam, Arresting failure propagation in buildings through collapse isolation, *Nat* 629 (8012) (2024) 592–596, <https://doi.org/10.1038/s41586-024-07268-5>.
- [14] F.-F. Feng, H.-J. Hwang, Y. Zhou, J.-M. Sun, H.-Z. Zhang, J.-H. Roh, S.-M. Kang, W.-J. Yi, Effect of three-dimensional space on progressive collapse resistance of reinforced concrete frames under various column removal scenarios, *J. Build. Eng.* 90 (2024) 109405, <https://doi.org/10.1016/j.job.2024.109405>.
- [15] D.-C. Feng, M.-X. Zhang, E. Brunesi, F. Parisi, J. Yu, Z. Zhou, Investigation of 3D effects on dynamic progressive collapse resistance of RC structures considering slabs and infill walls, *J. Build. Eng.* 54 (2022) 104421, <https://doi.org/10.1016/j.job.2022.104421>.
- [16] Y.-H. Weng, K. Qian, F. Fu, Q. Fang, Numerical investigation on load redistribution capacity of flat slab substructures to resist progressive collapse, *J. Build. Eng.* 29 (2020) 101109, <https://doi.org/10.1016/j.job.2019.101109>.
- [17] K. Qian, Y. Li, Review of study on progressive collapse resistance of RC structures, *J. Archit. Civ. Eng.* 39 (3) (2022) 1–28, <https://doi.org/10.19815/j.jace.2021.12123> (in Chinese).
- [18] Z. Li, Y. Liu, J. Huo, A.Y. Elghazouli, Experimental and analytical assessment of RC joints with varying reinforcement detailing under push-down loading before and after fires, *Eng. Struct.* 189 (2019) 550–564, <https://doi.org/10.1016/j.engstruct.2019.03.084>.
- [19] L. Jin, D.-Q. Lan, R.-B. Zhang, J. Li, K. Qian, Performance of RC beam-column assemblies during and after elevated temperature to resist progressive collapse, *Eng. Struct.* 283 (2023) 115802, <https://doi.org/10.1016/j.engstruct.2023.115802>.
- [20] J. Yu, T. Rinder, A. Stolz, K.-H. Tan, W. Riedel, Dynamic progressive collapse of an RC assemblage induced by contact detonation, *J. Struct. Eng.* 140 (6) (2014) 04014014, [https://doi.org/10.1061/\(ASCE\)ST.1943-541X.0000959](https://doi.org/10.1061/(ASCE)ST.1943-541X.0000959).
- [21] J. Sun, Y. Jia, Y. Yao, X. Xie, Experimental investigation of stress transients of blasted RC columns in the blasting demolition of buildings, *Eng. Struct.* 210 (2020) 110417, <https://doi.org/10.1016/j.engstruct.2020.110417>.
- [22] Z.-X. Li, H.-K. Liu, Y.-C. Shi, et al., Experimental study on progressive collapse mechanism of reinforced concrete sub-assemblage with two-span beams under blast loading, *J. Build. Struct.* 45 (1) (2024) 1–11, <https://doi.org/10.14006/j.jzjgxb.2023.0313> (in Chinese).
- [23] D.-C. Feng, S.-C. Xie, J. Xu, et al., Robustness quantification of reinforced concrete structures subjected to progressive collapse via the probability density evolution method, *Eng. Struct.* 202 (2022) 13, <https://doi.org/10.1016/j.engstruct.2019.109877>.
- [24] Y. Xiao, S. Kunnath, F.-W. Li, et al., Collapse test of three-story half-scale reinforced concrete frame building, *ACI Struct. J.* 112 (4) (2015) 429–438, <https://doi.org/10.14359/51687746>.
- [25] F. Yi, W.-J. Yi, J.-M. Sun, Y. Zhou, W.-X. Zhang, Q.-F. He, Experimental study on progressive collapse behavior of frame structures triggered by impact column removal, *Eng. Struct.* 321 (2024) 119022, <https://doi.org/10.1016/j.engstruct.2024.119022>.
- [26] X.-W. Cheng, Y. Li, X.-Z. Lu, et al., Numerical analysis of impact-induced collapse response of RC frames based on a multi-scale model, *J. Vib. Shock* 35 (5) (2016) 82–88, <https://doi.org/10.13465/j.cnki.jvs.2016.05.013> (in Chinese).
- [27] H. Kang, J. Kim, Progressive collapse of steel moment frames subjected to vehicle impact, *J. Perform. Constr. Facil.* 29 (6) (2015) 04014172, [https://doi.org/10.1061/\(ASCE\)CF.1943-5509.0000665](https://doi.org/10.1061/(ASCE)CF.1943-5509.0000665).
- [28] F. Yi, W.-J. Yi, J.-M. Sun, J. Ni, Q.-F. He, Y. Zhou, On the progressive collapse performance of RC frame structures under impact column removal, *Eng. Struct.* 307 (2024) 117926, <https://doi.org/10.1016/j.engstruct.2024.117926>.
- [29] Y.-C. Shi, Z.-X. Li, H. Hao, A new method for progressive collapse analysis of RC frames under blast loading, *Eng. Struct.* 32 (6) (2010) 1691–1703, <https://doi.org/10.1016/j.engstruct.2010.02.017>.
- [30] Y.-C. Shi, R. Jiang, Z.-X. Li, Y. Ding, A substructure based method for damage assessment of RC frame structures under close-in explosion, *Eng. Struct.* 272 (2022) 115017, <https://doi.org/10.1016/j.engstruct.2022.115017>.
- [31] P.S. Symonds, T.J. Mentel, Impulsive loading of plastic beams with axial constraints, *J. Mech. Phys. Solid.* 6 (3) (1958) 186–202, [https://doi.org/10.1016/0022-5096\(58\)90025-5](https://doi.org/10.1016/0022-5096(58)90025-5).
- [32] C. Demartino, J. Wu, Y. Xiao, Experimental and numerical study on the behavior of circular RC columns under impact loading, *Procedia Eng.* 199 (2017) 2457–2462, <https://doi.org/10.1016/j.proeng.2017.09.386>.
- [33] L. Chen, H. Wu, Q. Fang, R. Li, Full-scale experimental study of a reinforced concrete bridge pier under truck collision, *J. Bridge Eng.* 26 (8) (2021) 05021008, [https://doi.org/10.1061/\(ASCE\)BE.1943-5592.0001749](https://doi.org/10.1061/(ASCE)BE.1943-5592.0001749).
- [34] R.W. Li, D.Y. Zhou, H. Wu, Experimental and numerical study on impact resistance of RC bridge piers under lateral impact loading, *Eng. Fail. Anal.* 109 (2020) 104319, <https://doi.org/10.1016/j.engfailanal.2019.104319>.
- [35] Y. Sha, H. Hao, Laboratory tests and numerical simulations of CFRP strengthened RC pier subjected to barge impact load, *Int. J. Struct. Stabil. Dynam.* 15 (2) (2015) 1450037, <https://doi.org/10.1142/S0219455414500370>.
- [36] W. Fan, B. Liu, G.R. Consolazio, Residual capacity of axially loaded circular RC columns after lateral low-velocity impact, *J. Struct. Eng.* 145 (6) (2019) 04019039, [https://doi.org/10.1061/\(ASCE\)ST.1943-541X.0002324](https://doi.org/10.1061/(ASCE)ST.1943-541X.0002324).

- [37] J. Cai, J.-B. Ye, Q.-J. Chen, X. Liu, Y.-Q. Wang, Dynamic behaviour of axially-loaded RC columns under horizontal impact loading, *Eng. Struct.* 168 (2018) 684–697, <https://doi.org/10.1016/j.engstruct.2018.04.095>.
- [38] Y. Zhou, J. Yang, X. Luo, H.-J. Hwang, H. Chen, J. Sun, W. Yi, S.-M. Kang, Pendulum impact loading tests of precast concrete columns with various column base connections, *Eng. Struct.* 252 (2022) 113736, <https://doi.org/10.1016/j.engstruct.2021.113736>.
- [39] Y. Zhou, T. Chen, Y. Pei, H.-J. Hwang, X. Hu, W. Yi, L. Deng, Static load test on progressive collapse resistance of fully assembled precast concrete frame structure, *Eng. Struct.* 200 (2019) 109719, <https://doi.org/10.1016/j.engstruct.2019.109719>.
- [40] Y. Tian, Y. Su, Dynamic response of reinforced concrete beams following instantaneous removal of a bearing column, *Int. J. Concr. Struct. Mater.* 5 (1) (2011) 19–28, <https://doi.org/10.4334/IJCSM.2011.5.1.019>.
- [41] H. Sezen, K.J. Elwood, A.S. Whittaker, K.M. Mosalam, J.W. Wallace, J.F. Stanton, *Structural Engineering Reconnaissance of the August 17, 1999 Earthquake: Kocaeli (Izmit), Turkey Earthquake*, Pacific Earthquake Engineering Research Center, University of California, Berkeley, CA, USA, 2000.
- [42] Y. Zhou, X. Hu, Y. Pei, H.-J. Hwang, T. Chen, W. Yi, L. Deng, Dynamic load test on progressive collapse resistance of fully assembled precast concrete frame structures, *Eng. Struct.* 214 (2020) 110675, <https://doi.org/10.1016/j.engstruct.2020.110675>.
- [43] B.A. Izzuddin, A.G. Vlassis, A.Y. Elghazouli, D.A. Nethercot, Progressive collapse of multi-storey buildings due to sudden column loss—Part I: simplified assessment framework, *Eng. Struct.* 30 (5) (2008) 1308–1318, <https://doi.org/10.1016/j.engstruct.2007.07.011>.
- [44] A.G. Vlassis, B.A. Izzuddin, A.Y. Elghazouli, D.A. Nethercot, Progressive collapse of multi-storey buildings due to sudden column loss—Part II: application, *Eng. Struct.* 30 (5) (2008) 424–438, <https://doi.org/10.1016/j.engstruct.2007.08.011>.
- [45] K. Qian, J.-F. Cheng, Y.-H. Weng, F. Fu, Effect of loading methods on progressive collapse behavior of RC beam-slab substructures under corner column removal scenario, *J. Build. Eng.* 44 (2021) 103258, <https://doi.org/10.1016/j.job.2021.103258>.
- [46] K. Qian, Z. Li, Y.-H. Weng, X.-F. Deng, Behavior of RC beam-slab substructures to resist progressive collapse, *Eng. Mech.* 36 (6) (2019) 239–247, <https://doi.org/10.6052/j.issn.1000-4750.2018.05.0297> (in Chinese).
- [47] J.-F. Cheng, Q. Gu, K. Qian, F. Fu, X.-F. Deng, Dynamic behavior of RC frames against progressive collapse subjected to loss of a corner column scenario, *J. Build. Eng.* 86 (2024) 108872, <https://doi.org/10.1016/j.job.2024.108872>.
- [48] J. Yu, L. Luo, Y. Li, Numerical study of progressive collapse resistance of RC beam-slab substructures under perimeter column removal scenarios, *Eng. Struct.* 159 (2018) 14–27, <https://doi.org/10.1016/j.engstruct.2017.12.038>.
- [49] Y.D. Murray, *Users Manual for LS-DYNA Concrete Material Model 159*, Office of Research, Development and Technology, Federal Highway Administration, USA, 2007.
- [50] Y.D. Murray, A.Y. Abu-Odeh, R.P. Bligh, *Evaluation of LS-DYNA Concrete Material Model 159*, Office of Research, Development and Technology, Federal Highway Administration, USA, 2007.